Reports

Evidence for Magnetospheric Effects on the Sodium Atmosphere of Mercury

A. E. Potter and T. H. Morgan

Monochromatic images of Mercury at the sodium D_2 emission line showed excess sodium emission in localized regions at high northern and southern latitudes and day-to-day global variations in the distribution of sodium emission. These phenomena support the suggestion that magnetospheric effects could be the cause. Sputtering of surface minerals could produce sodium vapor in polar regions during magnetic substorms, when magnetospheric ions directly impact the surface. Another important process may be the transport of sodium ions along magnetic field lines toward polar regions, where they impact directly on the surface of Mercury and are neutralized to regenerate neutral sodium atoms. Day-to-day variations in planetary sodium distributions could result from changing solar activity, which can change the magnetosphere in time scales of a few hours. Observations of the sodium exosphere may provide a tool for remote monitoring of the magnetosphere of Mercury.

When we reported the discovery of sodium (Na) vapor in the atmosphere of Mercury (*1*), we noted that meteoritically driven processes (*2*) and ion sputtering were the most likely candidate processes for the production of Na. Since then, photon-stimulated desorption (*3*) and diffusion followed by thermal desorption (*4, 5*) have also been proposed as source processes, the effect of solar radiation pressure on the distribution of Na in the atmosphere of Mercury has been analyzed (*6, 7*), and the gross effect of radiation pressure on the total Na abundance has been observed (*8*). These processes have been discussed by Hunten *et al.* (*9*).

The various mechanisms proposed for supplying Na vapor to the Mercury atmosphere and their interactions with radiation pressure predict different distributions of Na about the sunlit hemisphere. It had been thought that measurements of spatial distributions of Na vapor would permit discrimination among these mechanisms. However, observations of the one-dimensional north-south and east-west distributions of Na have produced unexpected results (*10, 11*). Some of these observations suggest the existence of polar excesses of Na, and one data set showed daily variations of Na emission intensity. These effects are not predicted on the basis of the processes outlined above. In order to better understand these effects, we developed a method for obtaining two-dimensional images of the Na emission across the planet. We report here images obtained with this technique and present some suggestions about their significance.

Monochromatic images of Mercury were obtained simultaneously at the Na resonance lines and at a wavelength corresponding to surface-reflected sunlight by use of the McMath main solar telescope and stellar spectrograph of the National Solar Observatory at Kitt Peak, Arizona. The method of image production utilized a Bowen image slicer (*12*) coupled to a charge-coupled device (CCD) detector. The image slicer provided one spatial dimension, and the CCD detector elements provided the other (*13–15*). The combination produced a two-dimensional array of spectra, each of which we analyzed to determine the intensity of the Na emission and the surface-reflected continuum radiation, using procedures described in (*1, 6, 10*).

Because the angular size of the aperture of the image slicer was smaller than the angular size of Mercury, it was necessary to take two or more observations at different positions of Mercury on the slicer aperture, with a high-speed star tracker (*16*), to control the image position. Exposures were in the range 200 to 400 s. The images for which Mercury was at different positions on the slicer aperture were registered, with the continuum image used as a guide, and coadded to obtain a single image of the entire planet. The average standard deviation of Na emission intensity from one image to another was found to be 8% from analysis of three successive observations that overlapped the same region of the planet. The average standard deviation of the continuum intensity was much less, only a few percent, because the continuum signal was determined by integration of 40 spectral resolution elements. The blurring of the continuum image by atmospheric seeing and star-tracker jitter provided a measure of the effective seeing (full width at half maximum of the image of a point source), which was about 2 arc sec. The image at the D_2 resonance line (5890 Å) was always significantly better than the one at the D_1 resonance line (5896 Å), because of the approximate 2:1 ratio of emission intensities. As a result, only the D_2 images are presented in this report. Gradations in intensity in the images were normalized to the maximum intensity and reduced to eight bits, so that relative signal levels ranged from 0 (minimum) to 255 (maximum). For display, the intensity variations in the images were represented by shades of gray, which were later converted to false

Table 2. Approximate planetary locations of Na emission patches observed on Mercury. Emission patches did not appear on 11 November 1988, 16 February 1989, or 18 February 1989.

Date (1989)	North patch		South patch	
	Latitude (deg)	Longitude (deg)	Latitude (deg)	Longitude (deg)
17 February	60	350	50	350
7 July	60	270	50	330
23 August	60	170	50	170

Table 1. Configuration of Mercury at the times of image observations.

Date	Phase	Apparent diameter (arc sec)	Sub-Earth longitude (deg)	Distance from sun (AU)	Sodium Doppler shift (mÅ)
11 November 1988	0.928	5.14	168.1	0.3965638	190
16 February 1989	0.549	7.24	319.5	0.4393027	−124
17 February 1989	0.568	7.11	324.7	0.4429639	−116
18 February 1989	0.587	6.99	329.8	0.4463791	−108
07 July 1989	0.845	5.57	322.5	0.4653669	−95
23 August 1989	0.629	6.74	157.9	0.4660898	−25

A. E. Potter, Code SN3, National Aeronautics and Space Administration, Johnson Space Center, Houston, TX 77058.
T. H. Morgan, Code EL, National Aeronautics and Space Administration, Washington, DC 20546.

colors in order to better show differences.

Images of Mercury on 11 November 1988, 16 to 18 February 1989, 7 July 1989, and 23 August 1989 are shown in Figs. 1 through 4, respectively. Each figure shows an image of Mercury in the solar continuum reflected from the surface (left) and an image of Mercury in sodium D_2 emission (right). An outline drawing to the scale of the planet, showing the location of the terminator and the poles, is superimposed on each image. The configuration of Mercury (phase, apparent diameter, sub-Earth longitude, distance from the sun, and Doppler shift of the Na resonance line) for each observation is given in Table 1. The Na emission intensities quoted in the figure legends are the observed intensities and are a function of the Na vapor density, the distance of Mercury from the sun, and the Doppler shift of Mercury relative to the sun. For any one day (or series of days for which the solar distance and Doppler shift do not change significantly), the intensity of emission is a measure of the Na vapor density across the planetary disk.

These images show that (i) the distribution of Na is hardly ever symmetric about the luminance equator, (ii) there are major variations in the Na distribution from one day to the next, and (iii) on some days Na emission is concentrated in a pair of relatively small regions, one at a high north latitude and the other at a high south latitude. The approximate geographic locations of the bright emission regions are given in Table 2. These data show that there is a tendency for the northern patch to be at a higher latitude than the southern patch. The longitude of the patches was similar for the February and July observations, whereas the longitude for the August observations was almost 180° away from that for February and July. In some cases, the apparent size of the emission patch is not much larger than the effective spatial resolution of the measurement, which suggests that some of the bright emission areas may be less than an arc second in apparent size.

Can the physical processes that have been proposed to date (*1–8*) account for these observations? Impact vaporization driven by the flux of infalling micrometeoroids (*1, 2*) cannot account for polar concentrations of Na. Photon-stimulated desorption (*3*) also cannot account for polar concentrations of Na and would predict that the distribution always maximize around the subsolar point. Locally enhanced diffusion of Na out of the surface followed by thermal desorption (*4, 5*) can account for all kinds of nonuniform distributions of Na vapor, but it is difficult to explain rapid day-to-day changes unless volcanic activity is assumed. No evidence for recent vulcanism on Mercury can be seen in the Mariner 10 images. Radiation pressure effects (*6, 7*) also cannot account for the high-latitude bright regions and rapid changes in distribution. Although all these processes probably occur and must affect the Na atmosphere to varying degrees, it appears that some additional process must be at work to explain the observations outlined above. We suggest that this process is the flux of ions and electrons to the Mercury surface at high latitudes, producing neutral Na at the surface either by sputtering or by neutralization of Na^+.

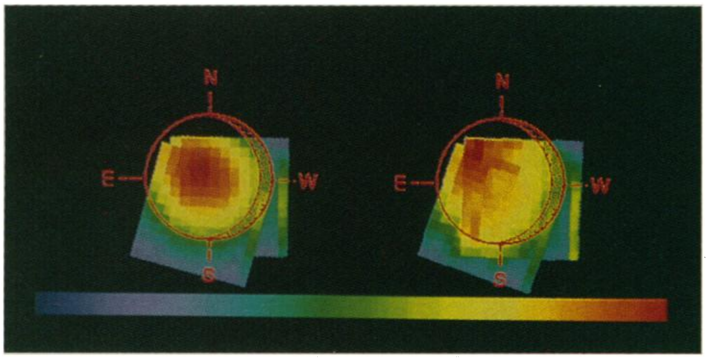

Fig. 1. Images of Na D_2 (right) and surface continuum reflection (left) for Mercury on 11 November 1988. The intensity values are represented by the color bar at the bottom. The continuum image was scaled such that red corresponded to the maximum continuum intensity. The Na emission intensity scale ran from 0.0 megarayleighs (MR) at the extreme left of the color bar (violet) to 2.8 MR at the extreme right of the bar (red). On this date, the planetary disk was almost fully illuminated, so that the subsolar point was nearly at the center of the disk. The Na D_2 image differs significantly from the continuum image. The Na emission is most intense away from the center of the disk and is concentrated in the northeast quadrant of the image. If the Na were uniformly distributed about the sunlit hemisphere, its emission would be symmetrical about the subsolar point near the center of the disk.

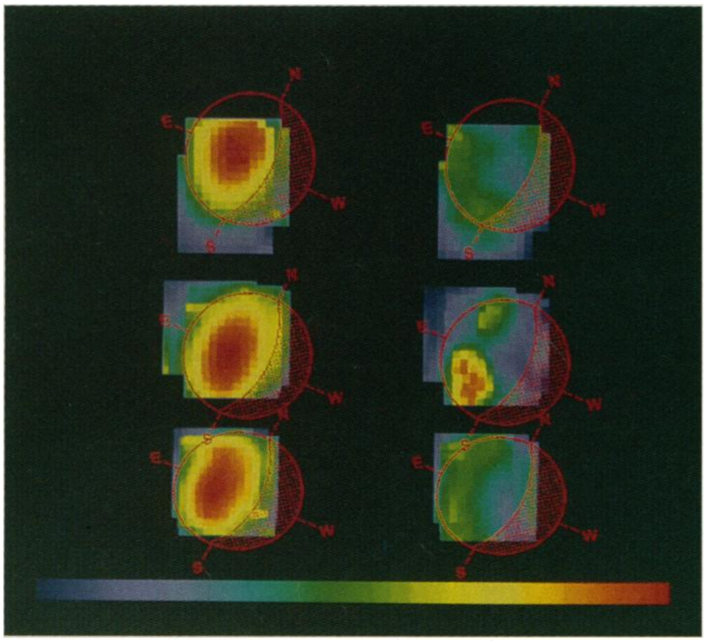

Fig. 2. Images of Na D_2 (right) and the surface continuum reflection (left) for Mercury for three consecutive days: 16 (top), 17 (center), and 18 (bottom) February 1989. The maximum Na intensity was set at 3.4 MR (red) for all three images in order to see more clearly the day-to-day changes. The planet was near maximum elongation for these observations. Examination of the 16 February Na D_2 image shows that the Na distribution along the bright limb is not uniform. The emission is peaked at the subsolar point, with lesser peaks away from the limb in southern and northern latitudes. The maximum emission intensity was 2.2 MR. On 17 February 1989, the distribution of Na emission about the apparent disk had changed. The Na emission is concentrated at a bright region in the lower portion of the image near the south pole of the planet, with a weaker emission region at a high northern latitude. The maximum emission intensity had increased to 3.4 MR. The observation on 18 February 1989 shows a simple limb-brightened Na image, which is expected for a uniform distribution of Na over the planet. The maximum emission intensity had dropped back to 2.2 MR. The magnitude of the day-to-day change from 16 to 17 February and from 17 to 18 February substantially exceeded the standard deviation of the measurement (estimated to be less than 10%). Observing conditions (good seeing, absence of clouds) were the same on all 3 days.

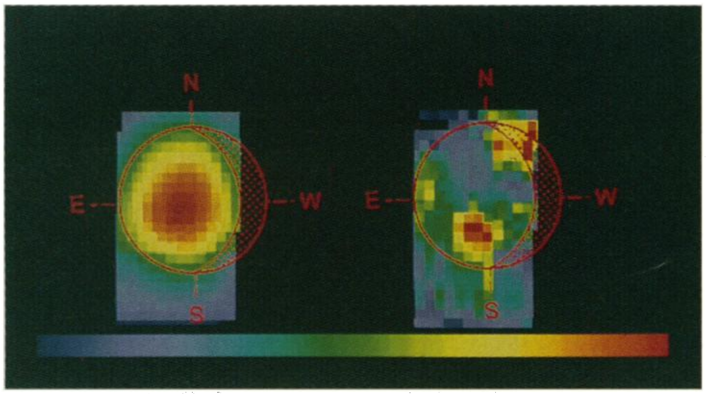

Fig. 3. Images of Na D_2 (right) and the surface continuum reflection (left) for Mercury on 7 July 1989. The maximum Na intensity was set at 3.8 MR (red). The Na emission was strongly peaked in northern and southern latitudes and was almost absent from the equatorial regions. This distribution is similar to that observed on 16 February but is more distinctly concentrated near the poles, with a maximum intensity of 3.8 MR at northern latitudes.

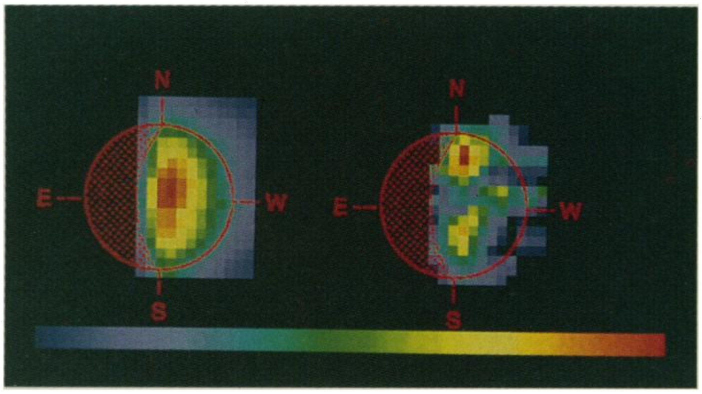

Fig. 4. Images of Na D_2 (right) and the surface continuum reflection (left) for Mercury on 23 August 1989. The maximum Na intensity was set at 1.2 MR (red). The Na emission pattern is similar to that seen in February and July, with emissions strongly peaked at a patch in northern latitudes and at another patch in southern latitudes. The maximum intensity was 1.2 MR, which was less than in the previous images because of the relatively low Doppler shift of the Na Fraunhofer line at the time of the observation.

Baker *et al.* (*17*) and Ip (*18*) have argued that considerable fluxes of magnetospheric ions and electrons may reach the surface at high latitudes during magnetic substorms, which may occur frequently on Mercury. The location of surface deposition is controlled by the magnetic field of the planet, such that these impact ovals would occur at similar north and south magnetic latitudes, but their extent and exact location would vary from day to day in response to changes at the field boundary resulting from changes in the solar wind. Baker *et al.* (*17*) estimated that the intensity of energy deposition in these ovals could reach 10^{14} W for periods of 10 s to several minutes. Substantial amounts of material could be sputtered from the surface during events of this intensity, which would provide a significant input of Na to the exosphere from high-latitude regions. In addition, the axis of the magnetic field may be as much as 20° from the planetary rotational axis, so that these zones would not be symmetric with respect to the luminance coordinates of the planet.

Another process leading to the generation of neutral Na atoms at high latitudes is the north-south transport of Na^+ in the planetary magnetic field (*10*). Atoms of Na have a lifetime of 1.4 to 3.3 hr before photoionization by solar ultraviolet radiation. The resulting ions will be caught in magnetic field lines and spiral north or south along the field lines until they contact the surface or are lost to space, depending on whether the lines are closed or open. Ions that contact the surface will be neutralized to regenerate Na atoms. This process will move Na toward the poles and will tend to concentrate it at high northern and southern latitudes. The effectiveness of this process will depend on the configuration of the planetary magnetic field, which is sensitive to the strength of the solar wind. Thus, the planetwide Na distribution could be indirectly affected by solar activity, as a consequence of its effect on the magnetosphere.

We conclude that sputtering of the surface by magnetospheric ions and latitudinal transport of Na^+ in the magnetosphere are the most likely processes responsible for (i) asymmetric distribution of Na with respect to the luminance equator, (ii) planetwide changes in the Na distribution over a time scale of a day, and (iii) regions of high Na concentration in symmetric north-south pairs. Further theoretical and observational work is needed to evaluate the relative importance of these two processes.

REFERENCES AND NOTES

1. A. Potter and T. Morgan, *Science* **229**, 651 (1985).
2. T. H. Morgan, H. A. Zook, A. E. Potter, *Icarus* **75**, 156 (1988).
3. M. A. McGrath, R. E. Johnson, L. J. Lanzerotti, *Nature* **323**, 694 (1986); A. F. Cheng, R. E. Johnson, S. M. Krimigis, L. J. Lanzerotti, *Icarus* **71**, 430 (1987).
4. A. L. Tyler, R. W. H. Kozlowski, D. M. Hunten, *Geophys. Res. Lett.* **15**, 1141 (1988).
5. R. M. Killen, *ibid.* **16**, 171 (1989).
6. W. H. Smyth, *Nature* **323**, 696 (1986).
7. J. Bishop and J. W. Chamberlain, *Icarus* **81**, 145 (1989).
8. A. E. Potter and T. H. Morgan, *ibid.* **71**, 472 (1987).
9. D. M. Hunten, T. H. Morgan, D. E. Shemansky, in *Mercury*, F. Vilas, C. R. Chapman, M. S. Matthews, Eds. (Univ. of Arizona Press, Tucson, 1988), p. 562.
10. R. M. Killen, A. E. Potter, T. H. Morgan, *Icarus*, in press.
11. A. L. Tyler, R. W. H. Kozlowski, N. H. Schneider, *Bull. Am. Astron. Soc.* **19**, 862 (1987).
12. K. Pierce, *Publ. Astron. Soc. Pac.* **77**, 216 (1965).
13. We produced images, using a Bowen image slicer (*12*) and a CCD detector, by the following procedure. The planet was focused at the entrance aperture of the slicer, which accepted a square area 5.2 arc sec on a side. The slicer optics dissected the planetary image into rectangular slices (five for measurements made before August 1989, ten for later measurements). Reflections inside the optics rearranged these elements, setting them end to end to form one long slice, which was equivalent in shape to the image of a single long slit. This composite slice passed through the stellar spectrograph and was refocused on the CCD detector, which was oriented so that each of the original image slices covered 12 CCD pixels. Each of these 12 then yielded a separate spectrum. Each of these spectra was from a different position on the slicer aperture, corresponding to a different position in the planetary image. We then analyzed each individual spectrum to yield values for the Na emission intensity and the reflected solar continuum intensity, using the procedure described in (*1*, *8*, *10*). Surface reflectivities for Mercury needed for the analysis were calculated from the procedures and data in (*14*, *15*). The values for Na emission intensity from each element were then assembled into two-dimensional

arrays at positions that matched their original positions at the entrance aperture of the Bowen slicer. These arrays were the sought-for monochromatic images of the planet. The image slicer used for this work had a 5.2 × 5.2 arc sec aperture. The slicer used before August 1989 provided a 5 × 12 array of 60 data points, each of which represented an angular area of 1.04 × 0.43 arc sec. The slicer used during August yielded 8 usable slices and an 8 × 12 array of 96 data points, each of which represented an angular area of 0.52 × 0.43 arc sec. For convenience in working with the data, we resampled the arrays to provide either a 12 × 12 or a 10 × 12 array (depending on which of the two slicers was used) of data points, each one corresponding to an angular area of 0.43 × 0.43 arc sec.

14. B. Hapke, *J. Geophys. Res.* **86**, 3039 (1981).
15. J. Veverka *et al.*, in *Mercury*, F. Vilas, C. R. Chapman, M. S. Matthews, Eds. (Univ. of Arizona Press, Tucson, 1988), p. 37.
16. The image stabilizer used for these observations was a DTI-221 high-speed video guider (Digital Television Imagery) and is a fourth generation of the "leaky memory guiders" used at Kitt Peak National Observatory.
17. D. N. Baker, J. E. Borovsky, J. O. Burns, G. R. Gisler, M. Zerlik, *J. Geophys. Res.* **92**, 4707 (1987).
18. W. H. Ip, *Geophys. Res. Lett.* **14**, 1191 (1988).
19. Both authors are visiting astronomers at the National Solar Observatory, operated by the Association of Universities for Research in Astronomy, Inc., under contract with the National Science Foundation. A.E.P. was supported by the National Aeronautics and Space Administration (NASA) Planetary Astronomy Program. T.H.M. was supported by the National Research Council. The authors acknowledge helpful comments from the referees, R. M. Killen, M. McGrath, J. Rahe, and H. Zook.

21 November 1989; accepted 7 March 1990

Identification of the Products from the Reaction of Chlorine with the Silicon(111)-(7×7) Surface

JOHN J. BOLAND AND J. S. VILLARRUBIA*

The various products from the reaction of chlorine (Cl) with the adatom layer of the Si(111)-(7×7) surface have been identified with scanning tunneling microscopy (STM). Initially, a single Cl atom reacts with the adatom dangling bond. At higher surface coverage, additional Cl atoms insert themselves into the Si–Si backbonds between the adatom and rest-atom layers, producing adatoms that have reacted with two or three Cl atoms. These products are characterized by different registries with respect to the underlying rest layer and appear in STM images as adatoms of different sizes, consistent with the breaking of Si–Si backbonds and the formation of new Si–Cl bonds.

SCANNING TUNNELING MICROSCOPY has developed into a powerful tool for the study of surfaces. The strength of STM lies in its ability to resolve, both in energy and real space, the electronic states of the surface within some energy window about the Fermi level E_f (*1*). Clean and adsorbate covered surfaces, in addition to thin overlayers, have been studied. Simple nondissociative adsorbates are identified on the basis of their known structural and electronic properties (*2*). Frequently, however, surface-adsorbate interactions involve significant bond making and breaking that result in the formation of a variety of different surface species. Although the presence of such species may be inferred spectroscopically, the ability of STM to identify the different products from a surface chemical reaction has yet to be established.

In this report we show that it is possible to distinguish between the various products from the reaction of Cl with the adatom layer of the Si(111)-(7×7) surface. These products, which correspond to three different Si adatom oxidation states, are characterized by different registries with respect to the underlying rest layer to which they are bonded. Furthermore, the different products are observed as adatoms of different sizes which is shown to be consistent with the breaking of successive Si–Si backbonds and the formation of new Si–Cl bonds.

The STM used in this work is similar to that described by Demuth *et al.* (*3*) and was mounted in an ion-pumped vacuum chamber with a base pressure of $\sim 1 \times 10^{-10}$ torr. The (7×7) surface was generated by heating a phosphorus-doped (1 ohm-cm) Si(111) wafer to 1050°C for 30 s. The Cl source was a AgCl electrochemical cell (*4*). The data shown consist of standard STM topographs in which the tunneling bias refers to the voltage on the sample.

The Si(111)-(7×7) surface adatom layer consists of triangular subunits that each contain six Si adatoms arranged locally in a (2×2) structure (*5*). These adatoms lie along or parallel to lines that bisect the triangular subunits of the cell. Each Si atom in the adatom layer has three backbonds to the Si atoms in the rest layer beneath and is situated in the threefold hollow formed by these rest atoms. The remaining Si adatom bonding orbital constitutes the adatom dangling bond (db), which point into the vacuum. In the present context the term adatom refers to the Si atoms in the adatom layer and not to the Cl atoms that subsequently react with this layer.

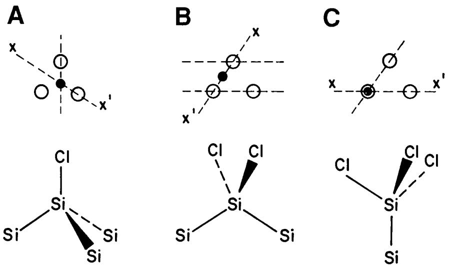

Fig. 1. Schematic showing the three possible reaction products. (**A**) SiCl, (**B**) $SiCl_2$, and (**C**) $SiCl_3$. The (111) surface is defined by the three rest atoms (○). The dashed lines correspond to the lines shown in Figs. 2 and 3. The top view (upper panel) shows the positions of all three rest atoms and the Si adatom, whereas the side view (lower panel) shows the Cl atoms and only the rest atoms that remain bonded to the adatom.

In an earlier report (*6*) we showed that at low surface coverages the Cl primarily interacts with the adatom db state and results in it occupying a site directly above the Si adatom. Therefore, adatoms that have reacted with a single Cl atom do not shift their positions from that of the unreacted surface and are situated in threefold hollow sites (Fig. 1A). As the coverage increases the Cl penetrates the relatively open adatom structure and inserts itself in one of the three backbonds between the adatom and the atoms in the rest layer beneath. Under saturation conditions, the rest atom db produced by this bond breaking is tied up by Cl. The reaction of the adatom with this additional Cl atom causes it to flip up out of the threefold hollow site and into a position where it is equidistant between the two remaining rest atoms to which it is bonded, lying along the line connecting these atoms in a bridge-bonding configuration (Fig. 1B). The reaction of a further Cl atom results in the breaking of one of these two backbonds, with the adatom now occupying an atop site directly above the remaining rest atom to which it is bonded (Fig. 1C).

X-ray photoelectron spectroscopy shows that all three adatom species are present after a room-temperature saturation dose of the surface (*7*). However, after a 400°C anneal the monochloro species predominates (*7*). Recently, we showed that this annealing process is associated with the transformation of an initially disordered (7×7) adatom structure to one in which the adatoms are stripped from the surface and accumulated

---

IBM Research Division, Thomas J. Watson Research Center, Yorktown Heights, NY 10598.

*Present address: National Institute of Standards and Technology, Gaithersburg, MD 20899.